Chinese Journal of Aeronautics, (2020), 33(10): 2707–2715

Chinese Society of Aeronautics and Astronautics
& Beihang University

Chinese Journal of Aeronautics

cja@buaa.edu.cn
www.sciencedirect.com

Control failure of the roll-isolated inertial navigation system under large pitch angle

Jinchao SONG [a,c], Shuxing YANG [a,b,c,*], Fenfen XIONG [a,c]

[a] School of Aerospace Engineering, Beijing Institute of Technology, Beijing 100081, China
[b] Xi'an Modern Control and Technology Institute, Xi'an 710065, China
[c] Key Laboratory of Dynamics and Control of Flight Vehicle, Ministry of Education, Beijing 100081, China

Received 26 October 2018; revised 23 December 2018; accepted 10 April 2019
Available online 11 October 2019

KEYWORDS

Spinning vehicle;
Strap-down inertial navigation system (SINS);
Roll-isolated control;
Control failure;
Large pitch angle

Abstract Roll-isolation is an effective way for spinning vehicle to greatly reduce the roll gyro range of strapdown Inertial Navigation System (SINS) and increase the accuracy of inertial navigation. However, during a recent flight test, the roll-isolated control system failure was observed under a large pitch angle ($70^\circ \leqslant \theta \leqslant 85^\circ$), which introduces a sharply increase in the roll angular velocity, the saturation of roll gyro and the inertial navigation failure. To address this issue, the governing equation of the roll-isolated system is derived with the consideration of various disturbance factors. The control failure is reproduced by numerical simulation. And the results show that the pitch and yaw angular velocity can cause a dramatic increase in roll rate under the large pitch angle, resulting in the roll-isolated control failure. Meanwhile, an improved roll-isolated control system is developed using PI controller, which is verified by mathematical simulation.

1. Introduction

A spinning vehicle spins around its longitudinal axis continuously during flight, which can reduce the impact of aerodynamic asymmetry, thrust eccentricity and other manufacturing errors, and only needs 1-2 control channels, which can simplify the control system composition.[1–7] Therefore, the spinning has been widely applied to miniaturized and low-cost flight vehicles. However, the continuous spinning of the vehicle with about 10 r/s, may cause problems such as increased range of the roll gyro and reduced navigation accuracy.[8–12] Hence, the application of the traditional strap-down inertial navigation system to the spinning vehicle is limited. To address this issue, various methods have been proposed. Imbault et al. proposed a roll-isolated strap-down inertial navigation technique with only one stable axis to isolate the continuous spinning of the vehicle,[13] with which the azimuth and pitch stabilized axes of the platform were eliminated based on the three-axis stabilized platform, and only the stabilization loop of roll maneuver is retained. Basically, the platform does not spin or only spins at a low roll angular velocity relative to the inertial space, in which only a stabilized axis is added based on the existing strap-down Inertial Measurement Unit (IMU). Therefore, it is also called the roll-isolated platform.[13-15] On

* Corresponding author.
E-mail address: yangshx@bit.edu.cn (S. YANG).
Peer review under responsibility of Editorial Committee of CJA.

https://doi.org/10.1016/j.cja.2019.08.026
1000-9361 © 2019 Chinese Society of Aeronautics and Astronautics. Production and hosting by Elsevier Ltd.

one hand, as the roll-isolated platform can isolate the vehicle spinning, the measuring device is not affected by the spinning of the vehicle, which dramatically reduces the range of the roll gyro.[16-18]On the other hand, the roll-isolated platform can significantly reduce the navigation error caused by the scale factor error of roll gyro, and improve the observability of the system as well[19]

However, in a recent flight test of spinning vehicle, the control failure of the roll-isolated SINS was observed under large pitch angle, resulting in the saturation of roll gyro, as shown in Fig. 1. With the increase of pitch angle (θ), especially when $\theta \geq$ 70 (°)/s, the roll-isolated control begins to fail, leading to a sharp increase in the roll angular velocity p (up to 150 (°)/s), and saturation of gyro with a range of 150 (°)/s.

In recent years, there are many literatures on the roll-isolated control system. Zhou et al. proposed a compensation method for roll-isolated optical fiber strap-down inertial navigation stable loop using the lead-lag network.[20] Later, they proposed a second-order discrete Active-Disturbance-Rejection Controller (ADRC) algorithm to effectively suppress the platform pedestal interference by employing the ADRC algorithm.[21] To improve the visibility and reduce alignment error, Shi et al. proposed a SINS calibration scheme for the initial position of the stationary base by changing the IMU roll angle around the roll axis based on the roll-isolated platform.[20] To address the issue that the slip ring is susceptible to electrical noise during transmission and then generates control errors in the harsh missile-borne environment, Liu et al. designed an active anti-rotation control method using servo motor.[22] Nonetheless, for almost all of the existing works, the roll-isolated control failure has not been mentioned yet, and the mechanism of the roll-isolated control failure under large pitch attitude angle has not been revealed. Therefore, it is the objective of this paper to make a comprehensive analysis of the reason for the roll-isolated control failure and propose the corresponding methods to deal with it.

The remainder of this paper is organized as follows. In Section 2, the model of roll-isolated control system is established. In Section 3, mechanism analysis for the roll-isolated control failure is presented. Improved control methods roll-isolated platform are proposed and verified in Section 4. Conclusions are drawn in Section 5.

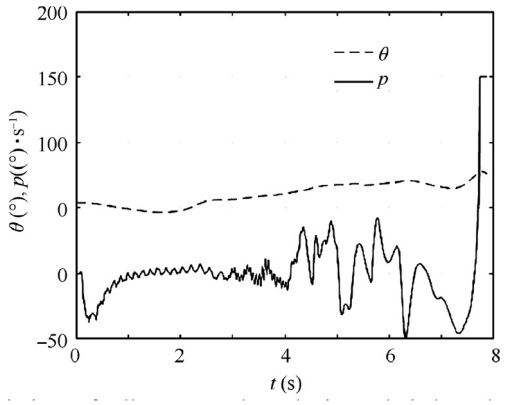

Fig. 1 Variations of roll gyro angular velocity and pitch angle with time.

2. Model of roll-isolated control system

2.1. Roll-isolated two-dimensional strap-down inertial navigation system

The roll-isolated two-dimensional Strap-down Inertial Navigation System (SINS) is originated from a three-axis stable platform with the elimination of the yaw and the pitch stable axis of the platform, and only the stabilization loop of the roll axis is retained, forming a roll-isolated platform with only one stable axis. In fact, the roll-isolated two-dimensional SINS is realized just by installing the classic SINS on the roll-isolated platform, as shown in Fig. 2.[20] For a roll-isolated stable platform with ideal roll-isolated support, the platform will not rotate with the spinning of carrier. However, the friction of the bearings will drive the platform to rotate with the spinning of carrier when the platform is supported by two bearings. A roll-isolated control system is constructed by means of the SINS, a torque motor and a controller to avoid the rotation of the platform. And the platform can keep stationary or spin at a very low roll rate relative to the inertial space. In some practical applications, the roll angle of the platform is used as the feedback due to the requirements on initial alignment and navigation accuracy, which indicates that the roll angle of the platform is almost zero. Therefore, the roll-isolated control system is mainly composed of PID controller, control motor, platform dynamics and SINS, as shown in Fig. 3.

2.2. Mathematical model of torque motor

Unlike the common motor position control system, the rotor of the motor fixed to the platform in the roll-isolated platform does not rotate, while the stator of the motor continuously rotates with spinning vehicle.

Fig. 4. shows an equivalent circuit diagram of the DC torque motor using the armature voltage control, where U_a is the armature control voltage, R_a is the armature resistance, L_a is the inductance, E_a is the counter electromotive force, i_a is the armature current, p_r is the angular velocity of motor output shaft relative to motor stator, T_L is the torque load of motor (friction, etc.).

The stator of the spinning vehicle motor that is fixed to the vehicle continuously rotates with the vehicle. Therefore, the stator roll angular velocity is equal to the vehicle roll angular velocity p_b, and the rotor roll angular velocity is equal to the platform roll angular velocity p. Then the relative roll angular velocity of the armature conductor in the stator magnetic field is

$$p_r = p - p_b \tag{1}$$

According to the principles of electromagnetics and physics, the equation of the rotating DC motor is obtained as follows.

Voltage balance equation:

$$U_a(t) = R_a i_a(t) + L_a \frac{di_a(t)}{dt} + E_a(t) \tag{2}$$

Induced electromotive force equation:

$$E_a(t) = k_E(p - p_b) \tag{3}$$

Electromagnetic torque equation:

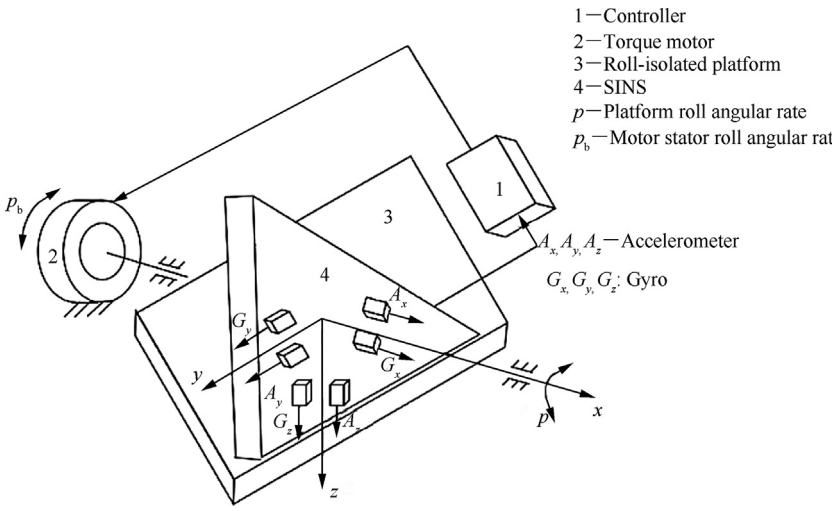

Fig. 2 Structure of roll-isolated two-dimensional SINS.

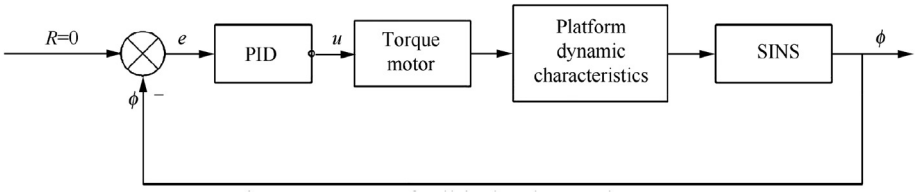

Fig. 3 Structure of roll-isolated control system.

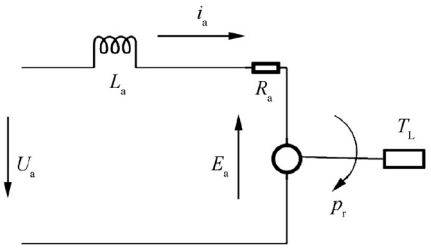

Fig. 4 Diagram of DC torque motor equivalent circuit.

$$T(t) = k_M i_a(t) \tag{4}$$

where k_E is the counter electromotive force coefficient and k_M is the electromagnetic torque coefficient.

2.3. Model of roll-isolated platform dynamics

The torque balance equation is

$$T(t) = J\frac{dp}{dt} + B \cdot p_r(t) + T_L(t) \tag{5}$$

where J is the inertial moment equivalent to the motor shaft; T_L is the torque load of motor (friction, etc.), B is the viscous damping coefficient equivalent to motor control shaft, and is often ignored.

The body coordinate system $oxyz$ is used to describe the dynamic model of the roll-isolated platform with the right-hand rule, where the coordinate origin is located at the centroid position of the vehicle, ox-axis coincides with the longitudinal axis of the vehicle, points to the direction of the nose, oy-axis is perpendicular to ox-axis in the reference plane of the vehicle and points right, oz-axis is perpendicular to oxy-plane and points down.

The three angular velocity components of the body coordinate system p, q and r are the components of the body axis system $oxyz$ angular velocity relative to the ground (inertia) coordinate system $ox_gy_gz_g$ respectively. The relationship between the body coordinate system and the ground coordinate system is shown in Fig. 5.

The body coordinate system $oxyz$ can be obtained by rotating yaw angle ψ, pitch angle θ and roll angle ϕ of the ground coordinate system $ox_gy_gz_g$ in the navigation calculation. First, transition coordinate system $ox'y'z_g$ is obtained by rotating ψ around oz_g-axis at the velocity of $\dot{\psi}$. Then, transition coordinate system $oxy'z'$ is obtained by rotating θ around oy'-axis

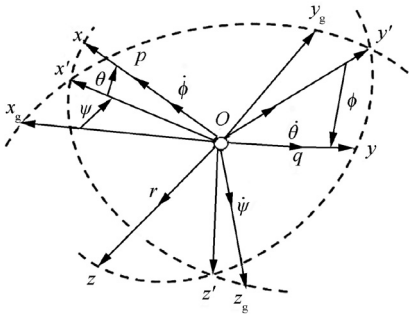

Fig. 5 Relationship between body coordinate system and ground axis system.

Table 1 Range of roll gyro needed of different pitch angle.

r((°)/s)	Range of roll gyro ((°)/s)				
	$\theta = 70°$	$\theta = 75°$	$\theta = 80°$	$\theta = 85°$	$\theta = 88°$
10	27.47	37.31	56.69	114.17	285.44
20	54.94	74.62	113.37	228.34	570.87
30	82.41	111.93	170.06	342.51	856.31

at the velocity of $\dot{\theta}$. At last, the body coordinate system $oxyz$ is obtained by rotating ϕ around ox-axis at the velocity of $\dot{\phi}$, which is common in the inertia navigation system (Table 1).

From Fig. 5, the relationship between the angular velocity component of the body coordinate system and the attitude angle rate can be obtained as follows.

$$\begin{cases} p = \dot{\phi} - \dot{\psi}\sin\theta \\ q = \dot{\theta}\cos\phi + \dot{\psi}\cos\theta\sin\phi \\ r = -\dot{\theta}\sin\phi + \dot{\psi}\cos\theta\cos\phi \end{cases} \tag{6}$$

Therefore, the attitude angle rate can be expressed as:

$$\begin{cases} \dot{\theta} = q\cos\phi - r\sin\phi \\ \dot{\psi} = \frac{1}{\cos\theta}(r\cos\phi + q\sin\phi) \\ \dot{\phi} = p + (r\cos\phi + q\sin\phi)\tan\theta \end{cases} \tag{7}$$

Clearly, the derivative of the platform roll angle can be expressed as:

$$\dot{\phi} = p + \tan\theta(r\cos\phi + q\sin\phi) \tag{8}$$

where p is the roll angular velocity of the platform/motor rotor, q and r are the gyro angular velocity along the pitch and yaw axis of platform respectively, θ is the pitch angle of vehicle and ϕ is the roll angle of platform. As the pitch and yaw channels of the platform are fixed to the vehicle, the pitch and yaw angular velocity of platform are equal to those of the vehicle, which can be measured by the SINS.

Denoted $k_r = \tan\theta\cos\phi$ and $k_q = \tan\theta\sin\phi$ respectively. Clearly, the disturbance factors k_r and k_q vary with ϕ and θ, and Eq. (8) can be rewritten as:

$$\dot{\phi} = p + k_r r + k_q q \tag{9}$$

2.4. PID control model of roll-isolated platform

As can be seen from Fig. 3, the PID controller of roll-isolated platform using ϕ as feedback can be written as:

$$U_a = -\left(k_P\phi + k_I\int\phi + k_D\dot{\phi}\right) \tag{10}$$

The transfer function Eqs. (11)–(13) can be obtained by using Laplace transformation on Eqs. (3), (5) and (10), with as the input, the roll angular velocity$p_b(s)$ pitch angular velocity $q(s)$, yaw angular velocity and torque load $T_L(s)$ of vehicle as the disturbance, and the roll angular velocity of platform as the output.

$$E_a(s) = k_E[p(s) - p_b(s)] \tag{11}$$

$$V(s) = U_a(s) - E_a(s) \tag{12}$$

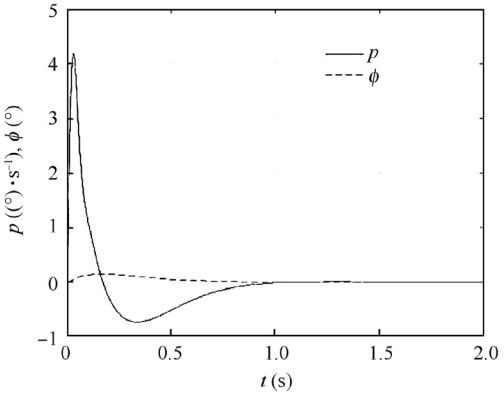

Fig. 7 Step response of roll angular velocity and roll angle of PID controller.

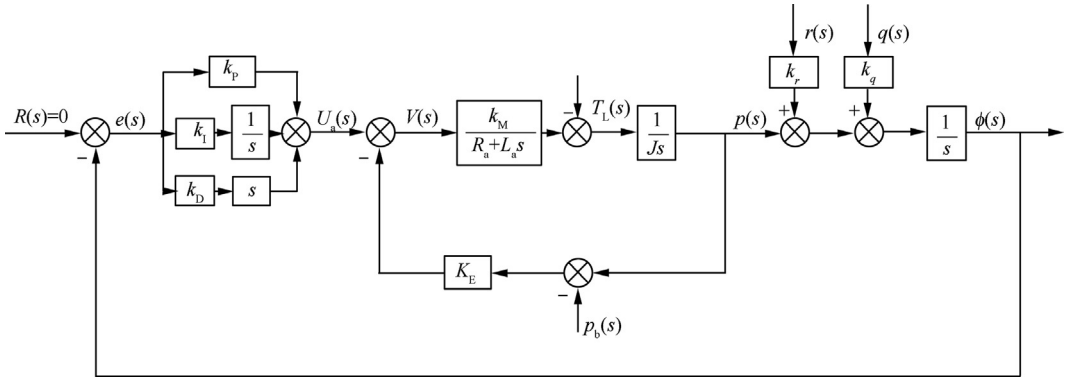

Fig. 6 Block diagram of roll-isolated PID control system.

$$p(s) = \frac{1}{Js}\left[V(s)\frac{k_M}{R_a + L_a s} - T_L(s)\right] \tag{13}$$

where and can be considered to be relatively constants under a definite pitch and roll attitude angle. By Laplace transformation of Eq. (9) one has

$$\phi(s) = \frac{1}{2}\left[p(s) + k_r r(s) + k_q q(s)\right] \tag{14}$$

The gains of the PID controller are denoted by k_P, k_I and k_D. One has

$$U_a(s) = -\left(k_P + \frac{k_I}{s} + k_D s\right)\phi(s) \tag{15}$$

Therefore, the block diagram of the roll-isolated control system can be obtained by Eqs. (13)–(15), as shown in Fig. 6.

3. Mechanism of the roll-isolated control failure

3.1. Fault recurrence of the roll-isolated control failure

Simulation is conducted for the roll-isolated platform control system under different pitch angle based on the mathematical model established in the previous section, in which the parameters of the motor are set as $R_a = 0.8\ \Omega$, $L_a = 0.0006$ H, $T_L = 0.2\ \mathrm{N \cdot m}$, $k_E = 4.94 \times 10^{-3}$ V/((°)/s),

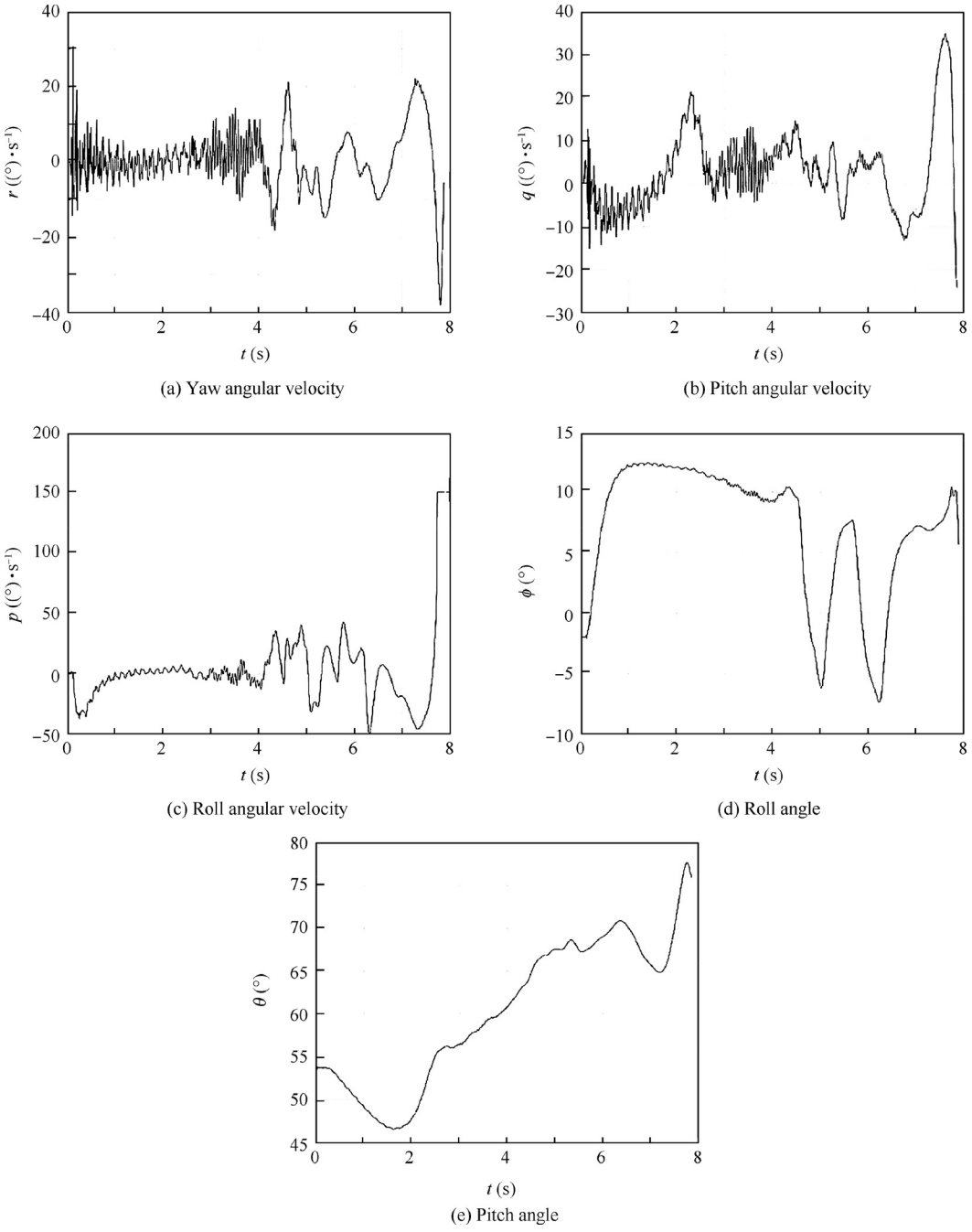

Fig. 8 Actual measurements of yaw angular velocity, pitch angular velocity, roll angular velocity, roll angle and pitch angle.

$k_M = 0.264\ \mathrm{N \cdot m/A}$, $J = 0.027\ \mathrm{kg \cdot m^2}$, and $p_b = 4469.4(°/s)$. And the parameters of the PID controller are $k_P = 80$, $k_I = 150$, $k_D = 10$ respectively.

The step responses of roll angular velocity roll angle of platform with pitch angle $\theta = 45^\circ$ and the roll angular velocity of the vehicle as step input (with amplitude 4469.4 (°)/s) are shown in Fig. 7. It is observed that when the roll angular velocity of the vehicle increases sharply, the roll angular velocity of the platform only varies at a low speed, while the roll angle of the platform is almost unchanged. Therefore, the roll-isolated control is effective.

Fig. 8 show the actual measurements of yaw angular velocity r, pitch angular velocity q, roll angular velocity p, roll angle pitch angle θ respectively.

By introducing the yaw angular velocity, pitch velocity and pitch angle obtained from the flight test, the evolution of the roll angular velocity with time is obtained. Fig. 9 shows the comparison between simulation and the flight test, where the full line p_{exp} denotes the roll angular velocity obtained from the test and the dotted line p_{pid} denotes the simulation result.

As shown in Fig. 9, both the roll-isolated control failure and the sharp increase in the roll angular velocity happen during simulation. After 7 seconds and the pitch angle exceeds 70°, the roll angular velocity increases sharply, and the roll-isolated control fails. When the roll angular velocity exceeds 150(°)/s, the range of the roll gyro during the test gets saturated and becomes ineffective. Due to model parameters and random interference during the test, the simulation and test results do not completely coincide with each other. However, they are consistent in trend.

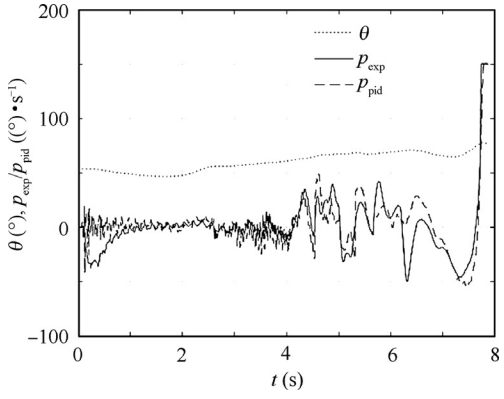

Fig. 9 Comparison of PID controller simulation results and measured data.

3.2. Mechanism of roll-isolated control failure

It can be seen from Fig. 6 that the roll-isolated control system has two disturbance terms, yaw angular velocity r and pitch angular velocity q. The surface diagram of the two disturbance term amplification factors k_r and k_q with respect to pitch angle θ roll angle ϕ shown in Fig. 10. It is observed that the amplification factors of the disturbance term k_r and k_q are increased with the increase of the pitch angle θ. Especially when the pitch angle θ is above 70°, k_r and k_q are increased significantly. Thus, some smaller disturbances in yaw angular velocity r and pitch angular velocity q can form a large strong input. This is the primary cause of the roll-isolated control failure.

Meanwhile, as shown in Fig. 10, when the roll angle is close to 0 deg, k_r, is larger, indicating that the yaw angular velocity is the main disturbance term. Similarly, when the roll angle is close to 90°, k_q is larger, indicating that the pitch angular velocity is the main disturbance term. During this flight test, as the roll angle is small (around 10°), the yaw angular velocity is the main disturbance. After about 7 s, a yaw angular velocity disturbance with the maximum magnitude of about 30 (°)/s occurs, resulting in the roll-isolated control failure.

Substitute Eq. (9) into Eq. (10), one can obtain the following equation:

$$U_a = -k_P\phi - k_I \int \phi - k_D(p + \tan\theta(r\cos\phi + q\sin\phi)) \qquad (16)$$

Clearly, the derivative element of the PID controller introduces additional disturbance inputs tan θ cos ϕ and tan θ sin ϕ q.

Fig. 11 shows the effect on roll angular velocity of PID and PI controller respectively, with $r = q = 30$ (°)/s. Evidently, the derivative element in the PID controller introduces additional disturbances, which aggravates the impact of yaw angular velocity and pitch angle, resulting in saturation of the roll gyro and failure of the roll-isolated platform ultimately.

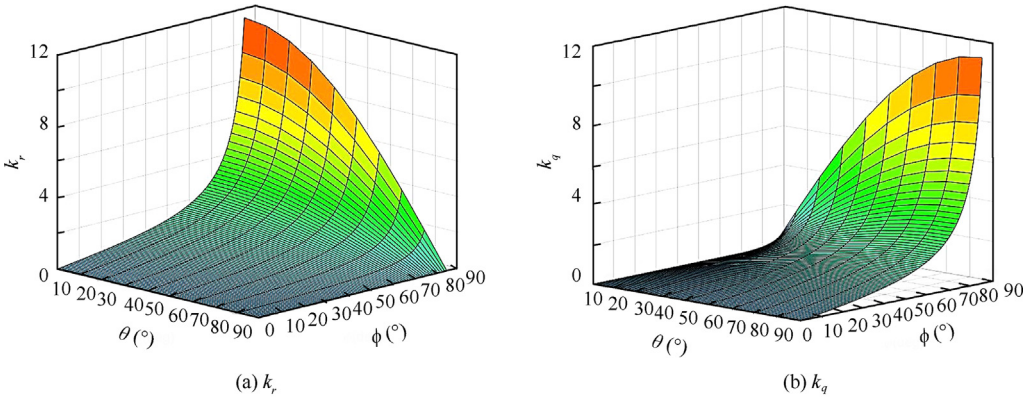

Fig. 10 Plot of disturbance term k_r and k_q.

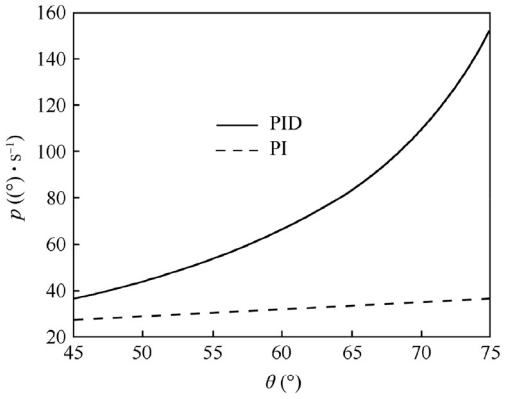

Fig. 11 Effect on roll angular velocity of PID and PI controller.

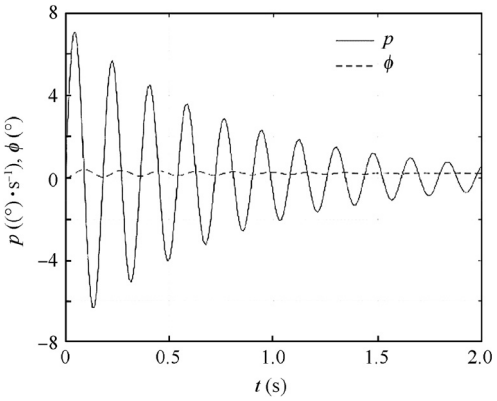

Fig. 13 Step response of roll angular velocity and roll angle of PI controller.

4. The improved roll-isolated platform control method

4.1. Roll-isolated control system without the derivative element

According to the analysis of the reason for the roll-isolated failure with large pitch angle in Section 3.2, it is noticed that the derivative element in the PID controller aggravates the roll-isolated control failure. To deal with this problem, the PID controller of the platform control model is changed into PI controller, as shown in Fig. 12. With a 4469.94 (°)/s step input of the vehicle's roll angular velocity p_b, the roll angular velocity p and roll angle q of the platform under pitch angle $\theta = 45^\circ$ are illustrated in Fig. 13, in which the parameters are the same as those in Section 3.1.

Obviously, once the derivative element is removed, the system damping is decreased and severe oscillation occurs. Therefore, an inner feedback loop of the roll angular velocity is introduced to increase the damping, as shown in Fig. 14.

The control parameter of the roll angular velocity feedback loop in the improved roll-isolated PI control system is set as $k_1 = 5$ and the other parameters are the same as those in Section 3.1. The parameters of the PI controller are set as: $k_P = 30$ and $k_I = 150$.

Simulation is conducted to verify the effectiveness of the PI control model. Fig. 15(a) shows the step responses of roll angular velocity p and the roll angle ϕ of the platform with pitch angle $\theta = 45^\circ$ and vehicle roll angular velocity p_b (amplitude 4469.94 (°)/s) as input. It is noticed that when the roll angular velocity of the vehicle varies rapidly, the roll angular velocity of the platform only varies slowly, indicating that the oscillation is effectively avoided. Moreover, the roll angle of the platform varies little, and the roll-isolated control is effective. Fig. 15(b) shows the step responses of roll angular velocity p and roll angle ϕ of the platform with pitch angle $\theta = 75^\circ$ and pitch and yaw angular velocity as inputs (amplitude 30 (°)/s). Apparently, the roll angular velocity is effectively reduced, and thus the roll-isolated control system can work well. Meanwhile, the roll gyro is not saturated, and the variation of the roll angle of the platform is small. Therefore, the improved roll-isolated control system is effective.

4.2. Roll-isolated control system using direct feedback of roll angular velocity

When the roll angle is not required to be zero during the initial alignment process, the roll angular velocity can also be directly fed back to form the roll-isolated control system. The block diagram is shown in Fig. 16.

Fig. 17 shows the roll angular velocity p and roll angle ϕ of the roll-isolated control system with direct feedback of the angular velocity, when the feedback loop control parameters are set as $k_2 = 5$ and pitch angle $\theta = 75^\circ$, and the pitch and yaw angular velocity step from zero to 30 (°)/s.

Compared with Fig. 15(b), with the same pitch angular velocity q and yaw angular velocity r disturbance, the

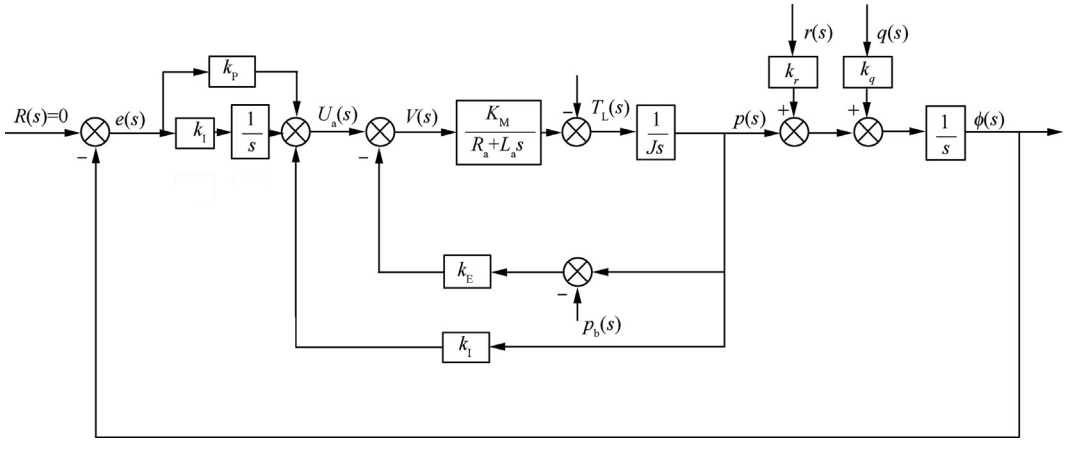

Fig. 12 Structure of the roll-isolated PI control system.

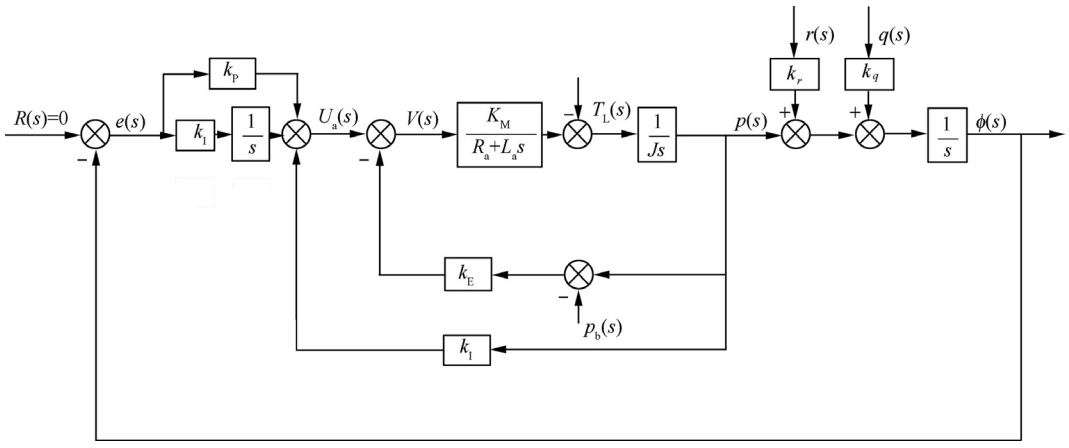

Fig. 14 Improved roll-isolated control system.

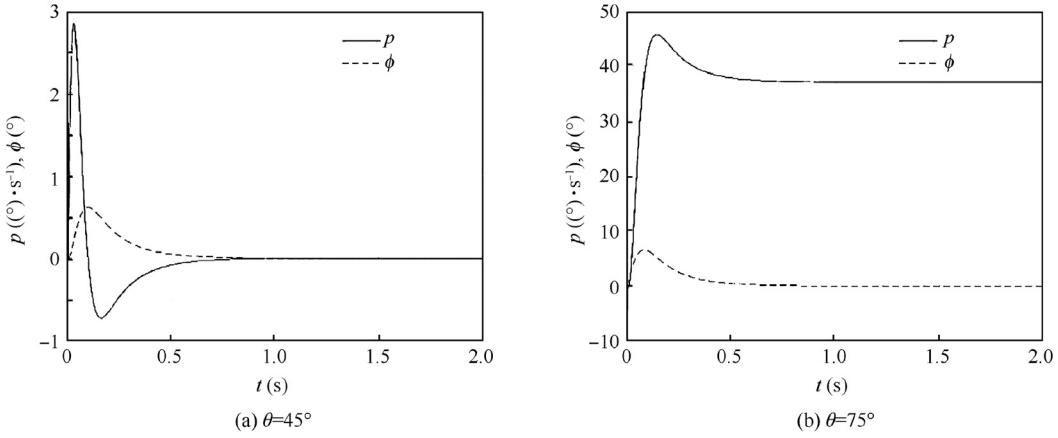

Fig. 15 Improved roll angle and roll angle step response.

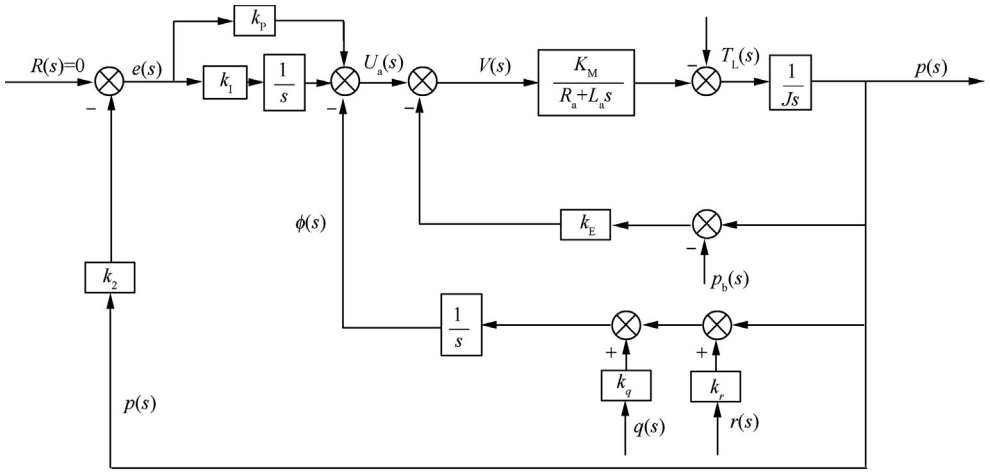

Fig. 16 Block diagram of the roll-isolated control system for direct feedback roll angular velocity.

variation of roll angular velocity p is smaller, while the roll angle ϕ increases continuously. Therefore, future research should focus on designing a strong anti-disturbance system, to stabilize both the roll angle and the roll angular velocity under large pitch and yaw angular velocity disturbance.

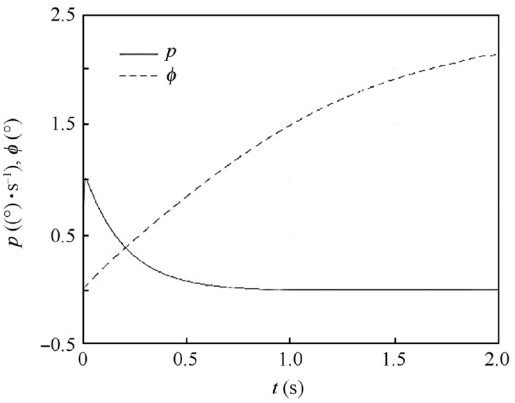

Fig. 17 Angular velocity curve of roll-isolated control system for direct feedback roll angular velocity.

5. Conclusion

This paper presents an analytical analysis of the control system of the roll-isolated SINS. The governing equation of the roll-isolated control system has been derived, considering various disturbance factors. It has been demonstrated that the pitch and yaw angular velocity can result in roll-isolation failure for the control system with the roll angle as the feedback under large pitch angle. It has been revealed that the large pitch angle can amplify the disturbance of the pitch and yaw angular velocity dramatically and result in failure of the roll-isolated control which induces saturation of the roll gyro range. Meanwhile, the derivative element in the PID controller is harmful and can introduce additional disturbance terms, which aggravates the disturbance of the pitch and the yaw angular velocity, and accelerates the failure of the roll-isolated control.

An improved scheme of the roll-isolated control system has been proposed, which eliminates the derivative element in PID controller and introduces a roll angular velocity feedback to increase the damping. Simulation results show that the scheme can reduce the disturbance effect of pitch and yaw angular velocity under large pitch angle to some extent, and reduce the possibility of the roll-isolated control failure. It has been also demonstrated that the only roll angular velocity feedback cannot stabilize the roll angle although it can eliminate the disturbance of the pitch and yaw angular velocity under the large pitch angle completely. Future research may focus on the architecture of strong anti-disturbance control system, which can effectively suppress the influence of pitch and yaw angular velocity disturbance and achieve roll angle control stability as well.

Acknowledgments

This study was co-supported by the National Science Foundation of China (No. 11532002) and Science Challenge Project of China (No. TZ2018001).

References

1. Yan XY, Yang SX, Zhang C. Coning motion of spinning missiles induced by the rate loop. *J Guidance Control Dyn* 2010;**33**(3):1490–9.
2. Yan XY, Yang SX, Xiong FF. Stability limits of spinning missiles with attitude autopilot. *J Guidance Control Dyn* 2011;**34**(1):278–83.
3. Li KY, Yang SX, Zhao LY. Stability of spinning missiles with an acceleration autopilo. *J Guidance Control Dyn* 2012;**35**(3):774–86.
4. Zhou W, Yang SX, Dong JL. Coning motion instability of spinning missiles induced by hinge moment. *J Guidance Control Dyn* 2013;**30**(1):239–45.
5. Hu X, Yang SX, Xiong FF, Zhang GQ. Stability of spinning missile with homing proportional guidance law. *Aerosp Sci Technol* 2017;**71**:546–55.
6. Zhao JB, Yang SX. Integrated cooperative guidance framework and cooperative guidance law for multi-missile. *Chin J Aeronau* 2018;**31**(3):546–55.
7. Zheng J, Dou LH, Xin B. A joint mid-course and terminal course cooperative guidance law for multi-missile salvo attack. *Chin J Aeronau* 2018;**31**(6):1311–26.
8. Schuler AR, Grammatikos A, Fegley KA. Measuring rotational motion with linear accelerometers. *IEEE Trans Aerosp Electron Syst* 1967;**3**(3):465–72.
9. Chen JH, Lee SC, DeBra DB. Gyroscope free strapdown inertial measurement unit by six linear accelerometers. *J Guidance, Control, Dyn* 1994;**17**(2):286–90.
10. Sungsu P, Chin WT, Joohyuk P. A Scheme for improving the performance of a gyroscope-free inertial measurement unit. *Sensors Actuators A: Physical* 2005;**121**(2):410–20.
11. Giovanni CS, Levinson E. Performance of a ring laser strapdown marine gyrocompass. *Navigation* 1981;**28**(4):311–41.
12. Shojiro I, Satoshi T, Hiroshi Y, Tadahiro H. Accuracy improvement of an inertial navigation system brought about by the rotational motion. Oceans 2007-Europe; 2007 June 18-21; Aberdeen, UK; 2007. p. 1–5.
13. James JI, Tjulin Hakan, Ragon K, Stewart K. Mini-RIMS-a miniature roll-stabilized inertial measurement system*AIAA conference on sounding rockets, ballons and related space systems; 1986 October 28–30*. Ocean City, MD, U.S.A. Reston: AIAA; 1986. p. 35–43.
14. Kim J, Choi HD, Lee JH. An anti-wind-up controller design for rocket control systems with control input saturation. *ImechE* 1998;**212**(4):261–9.
15. Mark EB. *Application of roll-isolated inertial measurement units to the instrumentation of spinning vehicles*. Albuquerque, New Mexico: Office of Scientific&Technical Information Technical Reports; 2000. p. 1–33.
16. Yang Z, Mo B, Nie Z. Design on MEMS based roll-isolated SINS in spinning projectile. *Telecom Market* 2013;**5**:46–51 [Chinese].
17. Li J, Zhao Y, Liu J, Chen W. Research on semi-strapdown MEMS inertial measurement device for flight attitude measurement of high-speed rotating ammunition. *Acta Armament* 2013;**34**(11):1398–403 [Chinese].
18. Li J, Liu J. Research on data transmission technology for rotating ammunition with semi-strapdown inertial measurement system. *J Projectiles Rockets Missiles&Guidance* 2014;**34**(4):57–60 [Chinese].
19. Shi Y, Wang B, Dong M, Gao Z. Research of roll-isolated gimbal platform and a two-position initial alignment scheme of SINS in spinning projectile. *Adv Mater Res* 2012;**383–390**:4115–20 [Chinese].
20. Zhou Q, Qin Y, Zhao C. Design on stabilization loop of roll-isolated SINS in spinning projectile. *J Chinese Inertial Technol* 2009;**17**(4):383–7 [Chinese].
21. Zhou Q, Qin Y, Yang P. Active Disturbance rejection control of the stabilizing loop for roll-isolated laser gyro strap down inertial navigation system. *Measur Control Technol* 2009;**28**(11):95–100 [Chinese].
22. Liu Y, Li J, Wang Y, Liu W, Zheng T. Design of the control system for axial anti-rotation platform used in rotating ammunition. *Chinese J Electron Dev* 2017;**40**(4):965–72 [Chinese].